Chinese Journal of Natural Medicines

Diphenylemestrins AE: diketopiperazine–diphenyl ether hybrids from *Aspergillus nidulans*

Aimin Fu, Qin Li, Yang Xiao, Jiaxin Dong, Yuanyang Peng, Yu Chen, Qingyi Tong, Chunmei Chen, Yonghui Zhang, Hucheng Zhu

Citation: Aimin Fu, Qin Li, Yang Xiao, Jiaxin Dong, Yuanyang Peng, Yu Chen, Qingyi Tong, Chunmei Chen, Yonghui Zhang, Hucheng Zhu, Diphenylemestrins AE: diketopiperazine–diphenyl ether hybrids from *Aspergillus nidulans*, Chinese Journal of Natural Medicines, 2025, 23(6), 727–732. doi: 10.1016/S1875–5364(25)60891–0.

View online: https://doi.org/10.1016/S1875–5364(25)60891–0

Chinese Journal of Natural Medicines 23 (2025) 727-732

Contents lists available at ScienceDirect

Chinese Journal of Natural Medicines

journal homepage: www.cjnmcpu.com/

Original article

Diphenylemestrins A–E: diketopiperazine-diphenyl ether hybrids from *Aspergillus nidulans*

Aimin Fu[Δ], Qin Li[Δ], Yang Xiao[Δ], Jiaxin Dong, Yuanyang Peng, Yu Chen, Qingyi Tong, Chunmei Chen[*], Yonghui Zhang[*], Hucheng Zhu[*]

Hubei Key Laboratory of Natural Medicinal Chemistry and Resource Evaluation, School of Pharmacy, Tongji Medical College, Huazhong University of Science and Technology, Wuhan 430030, China

ARTICLE INFO

Article history:
Received 23 October 2024
Revised 25 December 2024
Accepted 5 January 2025
Available online 20 June 2025

Keywords:
Chemical constituents
Biological activity
Aspergillus nidulans
Dioxopiperazines
Structure elucidation.

ABSTRACT

A chemical investigation of secondary metabolites (SMs) from *Aspergillus nidulans* resulted in the identification of five novel dioxopiperazine (DKP)-diphenyl ether hybrids, designated as diphenylemestrins A–E (**1**–**5**). These compounds **1**–**5** represent the first known dimers combining DKP and diphenyl ether structures, with compound **4** featuring an uncommon dibenzofuran as the diphenyl ether component. The structural elucidation and determination of absolute stereochemistry were accomplished through spectroscopic analysis and electronic circular dichroism (ECD) calculations. Notably, diphenylemestrin C (**3**) exhibited moderate cytostatic activity against NB4 cells, with a half maximal inhibitory concentration (IC_{50}) value of 21.99 μmol·L^{-1}, and induced apoptosis at higher concentrations.

1. Introduction

Aspergillus nidulans has served as a model organism for genetic and cellular biology studies over the past six decades. Chemical investigations have yielded the isolation of various compounds, including polyketides [1, 2], alkaloids [3-5], meroterpenoids [6, 7], and terpenes [8]. Several biosynthetic pathways for secondary metabolites (SMs) in *Aspergillus nidulans* have been elucidated, such as those for cichorine [9], *ent*-pimara-8(14),15-diene [8], aspernidine A [10], microperfuranone [11], aspernidulene A1 [12], and felinone A [13]. Whole genome sequencing and annotation have revealed that *Aspergillus nidulans* has the potential to produce a greater variety of SMs than previously identified [14, 15], as many biosynthetic genes are either silent or expressed at low levels under standard experimental conditions. Epipolythiodioxopiperazines (ETPs), typically characterized by a bridged polysulfide piperazine ring, exhibit a diverse range of bioactivities [16]. Emestrins, a subset of experimental environment. ETPs distinguished by a 15-membered macrocycle and at least one dihydrooxepine ring, were initially isolated from *Emericella striata* in 1986 [17]. To date, numerous emestrin analogues have been identified, with their unique structures and broad biological activities garnering significant scientific interest [17-21].

In our ongoing investigation of bioactive natural products from *Aspergillus nidulans* , various types of compounds have been isolated [22-25]. However, some trace SMs remained unidentified. This study employed large-scale fermentation to facilitate the discovery of additional trace SMs in *Aspergillus nidulans* [26, 27]. Five novel dioxopiperazines (DKPs) featuring a diphenyl ether moiety, named diphenylemestrins A–E (**1**–**5**), were isolated. Compounds **1**–**5** represent the first known dimers of DKP and diphenyl ether, with the diphenyl moiety in compound **4** exhibiting a rare dibenzofuran structure. This paper details the isolation, structural elucidation, and bioactivities of compounds **1**–**5**.

2. Results

Diphenylemestrin A (**1**) exhibited a molecular formula of $C_{41}H_{36}N_2O_{14}$, as determined by high resolution electrospray ionization mass spectroscopy (HR-ESI-MS) ion at *m/z* 803.2043 ([M + Na]$^+$, Calcd. for $C_{41}H_{36}N_2O_{14}Na^+$, 803.2064), indicating 25 degrees of unsaturation. The infrared (IR) spectrum revealed absorptions at 3420 and 1693 cm^{-1}, suggesting the presence of hydroxy and carbonyl groups. The ^{1}H nuclear magnetic resonance (NMR) data (Table S1) and ^{13}C NMR and Distortionless Enhancement by Polarization Transfer (DEPT) spectra (Table S2) indicated resonances for four methyls, including one *N*-methyl group (δ_H 3.11; δ_C 38.2) and one *O*-methyl group (δ_H 3.75; δ_C 55.3); 19 methines, including three oxygenated ones (δ_C 69.4, 72.3, and 79.5); three trisubstituted phenyl groups [δ_H 7.77 (d, *J* = 2.0 Hz), 7.42 (dd, *J* = 8.6, 2.0 Hz), 6.79 (d, *J* = 8.6 Hz); δ_H 7.02 (d, *J* = 2.0 Hz), 7.18 (dd, *J* = 8.5, 2.0 Hz), 7.00 (d, *J* = 8.5 Hz); δ_H 5.69 (t, *J* = 2.0 Hz), 5.72 (t, *J* = 2.0 Hz), 6,23 (t, *J* = 2.0 Hz)]; one tetrasubstituted phenyl group [δ_H 6.30 (d, *J* = 2.8 Hz), 6.54 (d, *J* = 2.8 Hz)]. The ^{13}C NMR displayed 41 carbon signals, which were assigned by DEPT and HSQC data as four methyl, 19 methines (14 olefinic and five sp^3-hybrid ones), and 18 quaternary (14 olefinic, three carbonyl,

* Corresponding author.
E-mail addresses: zhuhucheng@hust.edu.cn (H.Zhu); zhangyh@mails.tjmu.edu.cn (Y.Zhang); chenchunmei@hust.edu.cn (C.Chen)
Δ These authors contributed equally to this work.

https://doi.org/10.1016/S1875-5364(25)60891-0

and one sp^3-hybrid) carbon atoms. These signals of **1** resembled those of emestrin (Fig. S2) which characterized by the DKP core fused 3,4-dihydrooxepine through a pyrrolidine ring [28]. The heteronuclear multiple bond correlation (HMBC) (Fig. 2) from *N*-Me to C-1 and C-3, from H-5a to C-4 and C-10a, from H-10 to C-5a, C-8, and C-11, and from H-11 to C-5a and C-11a, combined with the ^{1}H–^{1}H correlation spectroscopy (COSY) spin system H-5a/H-6/H-7/H-8 indicated the ETP core. Additionally, the HMBC from H-6, H-2′, and H-6′ to C-7′ and H-7″ to C-3, C-4, C-2″, and C-6″ demonstrated the presence of a 15-membered macrolide. The remaining signal was characterized by ^{1}H NMR data of one trisubstituted and one tetrasubstituted phenyl groups, similar to diphenyl ether [29, 30]. The HMBC from H-12 to C-13, C-14, C-16, and C-17, from Me-18 to C-14, C-15, and C-16, from H-20 to C-19, C-21, C-22, and C-24, and from Me-25 to C-22, C-23, and C-24 confirmed the diphenyl ether moiety, analogous to quercilolin [31]. Lastly, the HMBC from OH-11 to C-10a, C-11, and C-11a, from OH-14 to C-14 and C-15, from OH-21 to C-20, C-21, and C-22, from OH-4″ to C-3″, C-4″, and C-5″, and from OH-7″ to C-3, C-1″, and C-7″ suggested the presence of OH-11, OH-14, OH-21, OH-4″, and OH-7″. The key nuclear Overhauser effect spectroscopy (NOESY) correlation of H-16 and H-24 confirmed C-17 connecting to C-19 through an ether bond, and the remaining one degree of unsaturation indicated C-11a connecting to C-13 through an ether bond.

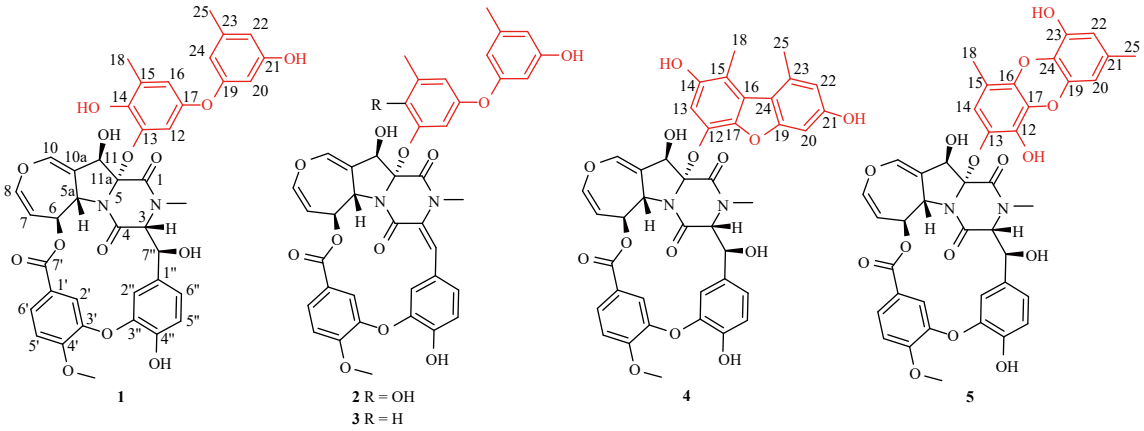

Fig. 1 Structures of **1–5**.

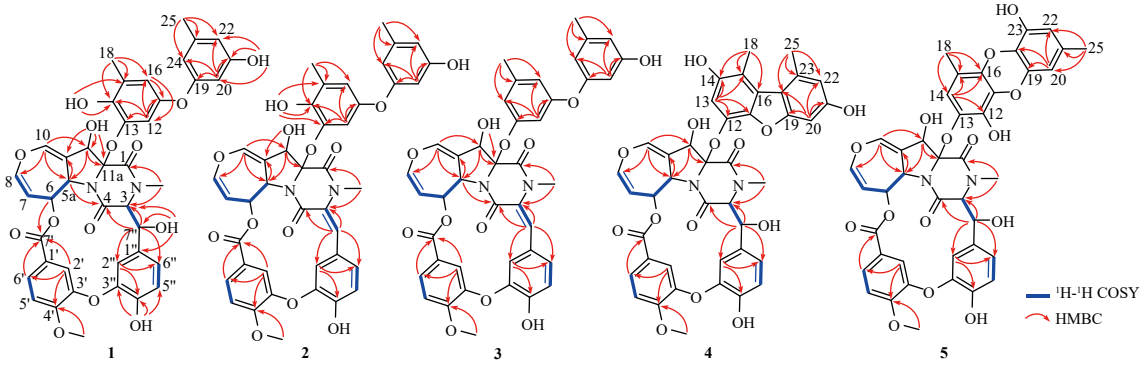

Fig. 2 Key ^{1}H–^{1}H COSY and HMBC correlations of compounds **1–5**.

The coupling constant (^3J = 8.4 Hz) between H-5a and H-6 in **1** indicated their *trans*-relationship [17, 28], with H-5a assigned a *β*-orientation. NOESY correlations of H-5a/OH-11, H-6/H-12, and H-12/H-7″ suggested a *β*-orientation for OH-11, while H-6 and H-7″ were *α*-oriented, and C-11a had an *R**relative configuration. Additionally, NOESY correlations of H-3/H-6″, H-12/H-7″, H-2″/H-7″, and H-6″/OH-7″ indicated a *β* -orientation for H-3 (Fig. 3). The dihedral angle between H-3 and H-7 ″ was approximately 180°, aligning with the observed coupling constant (^3J = 9.5 Hz). Two isomers, (3*R**, 5a*S**, 6*S**, 11*R**, 11a*R**, 7 ″ *S**)-**1** (**1a**) and (3*S**, 5a*S**, 6*S**, 11*R**, 11a*R**, 7″*S**)-**1** (**1b**), were proposed for further analysis. DP4$^+$ probability analysis revealed **1a** as the most probable structure, with a DP4$^+$ probability of 100% based on the ^{13}C NMR data (Table S4). The absolute configuration of **1** was determined by comparing the experimental and calculated electronic circular dichroism (ECD) spectra. The experimental ECD of **1** closely matched the calculated ECD curves of (3*R*, 5a*S*, 6*S*, 11*R*, 11a*R*, 7 ″ *S*)-**1** (Fig. 4), thereby unambiguously elucidating the structure of **1**.

Diphenylemestrin B (**2**) was isolated as a light yellow powder, and its molecular formula of $C_{41}H_{34}N_2O_{13}$ was determined from HR-ESI-MS at *m/z* 785.1966 [M + Na]$^+$ (Calcd. for $C_{41}H_{34}N_2O_{13}Na^+$, 785.1959), which was 18 mass units less than that of **1**. The ^{1}H and ^{13}C NMR data of **2** (Tables S1 and S2) were similar to those of **1**, with the notible exception of two additional olefinic carbons (δ_C 130.3 and 123.4) and the absence of two methines. The HMBC from *N*-Me to C-3, and from H-7″ to C-3, C-4, C-2″, and C-6″ indicated the double bond' location between C-3 and C-7″. The NOESY correlation of *N*-Me and H-7″ of **2** suggested the *E*-geometry of the $\Delta^{3(7'')}$ double bond. The coupling constant and NOESY spectrum revealed that the relative configuration of **2** was consistent with that of **1** (Fig. S17).

Diphenylemestrin C (**3**), a yellow powder, exhibited a molecular formula of $C_{41}H_{34}N_2O_{12}$ with 26 degrees of unsaturation, as determined by HR-ESI-MS at *m/z* 769.2031 [M + Na]$^+$ (Calcd. for $C_{41}H_{34}N_2O_{12}Na^+$, 769.2009), indicating one oxygen atom less than that of **2**. Analysis of the ^{1}H and ^{13}C NMR spectra revealed that the structure of **3** was nearly identical to **2**, with the primary difference being the presence of a trisubstituted phenyl [δ_H 5.94 (t, *J* = 2.3 Hz); 5.98 (t, *J* = 2.3 Hz); 6.29 (t, *J* = 2.3 Hz)] in **3** instead of a tetrasubstituted phenyl connected to C-11a in **2**. This struc-

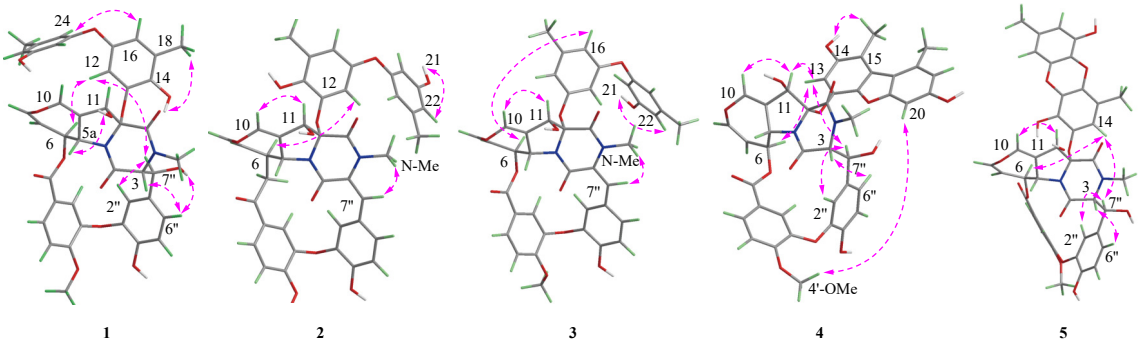

Fig. 3 Selected key NOESY correlations of compounds **1–5**.

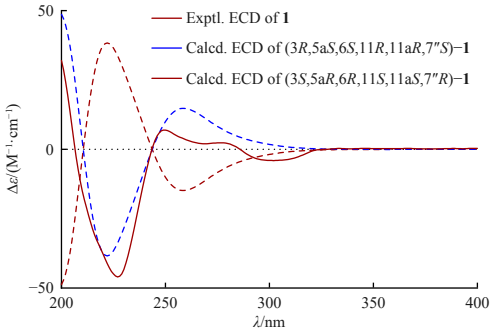

Fig. 4 Experimental and calculated ECD spectra of **1**.

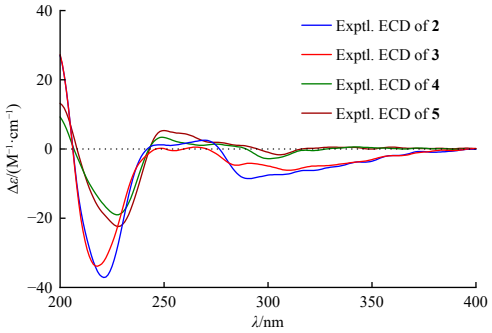

Fig. 5 Experimental ECD spectra of compounds **2–5**.

tural difference was corroborated by the HMBC from Me-18 to C-14, C-15, and C-16. The NOESY correlation between *N*-Me and H-7″ of **3** indicated the *E*-geometry of the $\Delta^{3(7'')}$ double bond. The coupling constant and NOESY spectrum of **3** confirmed that its relative configuration aligned with that of **2** (Fig. S26).

Diphenylemestrin D (**4**) was isolated as a yellow powder, with a molecular formula of $C_{41}H_{34}N_2O_{14}$ and 25 degrees of unsaturation, as determined by the molecular ion $[M + Na]^+$ peak at *m/z* 801.1891. The ^1H and ^{13}C NMR data (Tables S1 and S2) of **4** closely resembled those of **1** in the emestrin moiety, while the remaining signals were similar to diorcinol H, previously isolated from the endolichenic fungus *Aspergillus versicolor* [30]. The NOESY correlation of H-6/H-13 and H-13/H-7″, along with the HMBC from OH-14 to C-14 (recorded in DMSO-d_6, Table S3, Figure S39, and S41), indicated that etherification occurred at C-12. Analysis of $^1H–^1H$ coupling constants and NOESY signals suggested that **4** shares the same relative configuration as **1**.

Diphenylemestrin E (**5**) exhibited a molecular formula of $C_{41}H_{34}N_2O_{15}$, as determined by HR-ESI-MS (*m/z* 817.1876 $[M + Na]^+$, Calcd. for 817.1857), indicating 25 degrees of unsaturation. Comprehensive analysis of ^1H and ^{13}C NMR spectra of **5** revealed that its emestrin moiety was identical to that in **1**, while the remaining signals closely resembled those of gibellulin D [29]. Comparison of the NMR data between gibellulin D and gibellulin C suggested that a difference in etherified position significantly influenced the chemical shifts of two methyl groups [29]. Consequently, based on this comparison, the etherified position of **5** was determined to be C-13. The identical coupling constant between H-5a and H-6, along with NOESY correlations in **5** and **1**, indicated a shared relative configuration. Considering the likely similar biosynthetic origin of **2–5** with **1**, and in conjunction with the nearly identical ECD spectra of these compounds (Fig. 5), the absolute configurations of **2–5** were deduced as illustrated (Fig. 1).

In a previous study, emestrin derivatives demonstrated significant cytotoxicity against cancer cell lines [32, 33]. Consequently, compounds **1–5** were evaluated for their cytotoxicity against various cancer cell lines (NB4, RKO, A549, SU-DHL-2, HepG2, and HL60), with compound **3** exhibiting moderate cytostatic effects. The half maximal inhibitory concentration (IC_{50}) values of compound **3** against NB4 were 21.99 μmol·L^{-1} (24 h) and 18.86 μmol·L^{-1}(48 h), while the IC_{50} values for other cell lines were approximately 40μmol·L^{-1} . Subsequently, NB4 cells were utilized as a model to analyze the anti-cancer effects of compound **3**. A marked decrease in cell viability (Fig. 6A), notable cell shrinkage, and abundant cell debris after prolonged treatment suggested the apoptosis-inducing effect of compound **3** (Fig. 6B). As anticipated, after 24 h treatment with compound **3** (40 μmol·L^{-1}) and Etoposide (VP-16) (2 μmol·L^{-1}, positive control), the apoptosis rates of NB4 cells were 75.34% and 32.30%, respectively (Figs. 6C, 6D). However, apoptotic cells were not detected when treated with compound **3** at 20 μmol·L^{-1}, indicating a cytostatic effect rather than cytotoxicity or apoptosis induction at low concentrations (Figs. 6A, 6C, 6D). This further suggests a progressive action, with some early apoptosis-inducing events occurring. A decrease in mitochondrial membrane potential (a hallmark event in the early stages of apoptosis) was observed in NB4 cells following treatment with compound **3** (Figs. 6E, 6F). An increase in the green fluorescence of JC-1 monomers was also noted in NB4 cells *via* fluorescence microscopy. Moreover, compound **3** treatment induced the activation of caspase-3 and cleavage of poly (ADP-ribose) polymerase (PARP) (Fig. 6H), indicating the occurrence of apoptosis at the molecular level. In summary, the results demonstrated that compound **3** exhibited a cytostatic effect at low concentrations and an apoptosis-inducing effect at higher concentrations against NB4 cells.

3. Conclusion

In conclusion, the One Strain Many Compounds (OSMAC) approach, combined with a large-scale culture strategy, facilitated the isolation of five novel ether-bridged dimers of DKP and diphenyl ether, identified as diphenylemestrins A–E (**1–5**). Notably, diphenylemestrin C (**3**) demonstrated moderate cytostatic activity against NB4 cells and induced apoptosis at elevated concentrations.

4. Experimental

4.1. General experimental procedures

Optical rotations were measured using a Rudolph Autopol IV automatic polarimeter in MeOH (Rudolph Research Analytical, Hackettstown, NJ, USA). UV spectra were recorded on a SolidSpec-3700 instrument (Shimadzu, Kyoto, Japan). ECD spectra were obtained using a J-810 instrument (JASCO, Tokyo, Japan), and IR spectra were measured on a Nicolet iS50R FT-IR instrument (Thermo Scientific, Waltham, US). NMR spectra were acquired on a Bruker AM-400 NMR spectrometer and a Bruker AVANCE NEO 600 NMR spectrometer (Bruker, Karlsruhe, Germany). Chemical shifts (δ) were referenced to residual peaks for Methanol-d_4 (δ_H 3.31/δ_C 49.0), DMSO-d_6 (δ_C 39.52 and δ_H 2.50). HR-ESI-MS data were obtained on a microOTOF II instrument (Bruker, Karlsruhe, Germany). Column chromatography was performed using lichroprep reversed-phase C_{18} gel (Merck, Darmstadt, Germany), Sephadex LH-20 (Merck, Darmstadt, Germany), and silica gel (100–200 mesh, 200–300 mesh, Qingdao Marine Chemical, Inc., Qingdao, China).

4.2. Fungal material

Aspergillus nidulans was isolated from the Annelida *Whitmania pigra* Whitmana in Qichun, Hubei, China. A BLAST search revealed that its sequence was 99% identical to the sequence of *Aspergillus nidulans* (MH237626.1). The sequence data has been deposited in DDBJ/EMBL/GenBank under accession number MK39776.

4.3. Extraction and isolation

The seed of *Aspergillus nidulans* was cultivated on potato dextrose agar (PDA) at 25 °C for 10 days. The PDA was then distributed into 800 Erlenmeyer flasks (1 L) containing solid rice medium (250 g) and fermented at 25 °C for 45 days. The rice medium was extracted with EtOH at room temperature, after which the entire extract was suspended in H_2O and extracted with ethyl

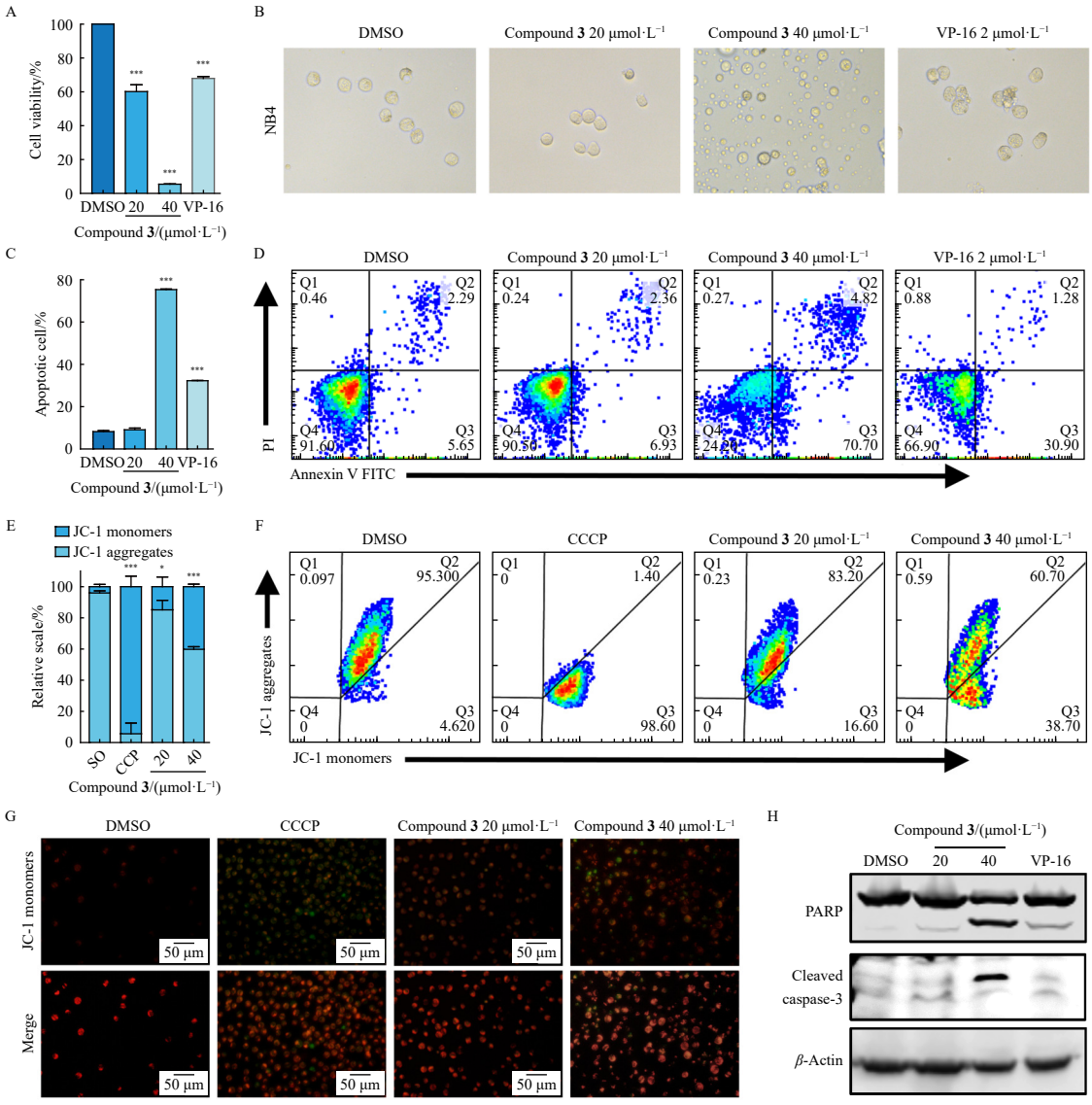

Fig. 6 Compound **3** treatment inhibited the proliferation of NB4 cells and induced apoptosis. (A) The viability of NB4 cells was evaluated using a CCK-8 Kit after treated with compound **3** for 24 h. (B) Morphological changes of NB4 cells after compound **3** treatment. (C, D) The apoptosis of NB4 cells was determined by Annexin V-FITC/PI Apoptosis Detection Kit after treatment with compound **3** for 24 h. (E, F, G) Mitochondrial membrane potential of NB4 cells was determined by flow cytometry and fluorescence microscope using a Mitochondrial Membrane Potential Assay Kit with JC-1. (E) Quantification of the percentage of JC-1 monomers/aggregates signal. (H) Western blot analysis of the expression of PARP, cleaved-caspase 3 proteins in NB4 cells after compound **3** treatment for 24 h. (A, C, E) The data was expressed as the mean ± SD of three independent experiments, $^{*}P < 0.1$, $^{**}P < 0.01$, $^{***}P < 0.001$ unpaired two-tailed Student's *t*-test. β-Actin was used as a loading control in western blot analysis.

acetate, yielding 1200 g of residue. The ethyl acetate fraction underwent silica gel column chromatography with gradient elution using petroleum ether/ethyl acetate/methanol (10 : 1 : 0, 8 : 1 : 0, 5 : 1 : 0, 3 : 1 : 0, 1 : 1 : 0, 1 : 1 : 0.1, *V/V*) to produce seven subfractions (A–G). Fr. E (34.09 g) was eluted on a reversed-phase C_{18} column with MeOH–H_2O (20%–100%) to yield seven fractions (E1–E7). The E4 fraction was eluted with a silica gel column using CH_2Cl_2–MeOH (100 : 0 to 10 : 1, *V/V*) to afford six fractions (E4a–E4f). The E4c fraction was eluted on a Sephadex LH-20 column (MeOH : CH_2Cl_2 = 1 : 1) to produce five fractions (E4c1–E4c5). Fr. E4c4 was eluted on a reversed-phase C_{18} column with MeOH–H_2O (40%–80%) and subsequently purified with a silica gel column to yield **1** (29.3 mg). The E4d fraction was eluted on a Sephadex LH-20 column (MeOH : CH_2Cl_2 = 1 : 1) to afford 5 fractions (E4d1–E4d5). Fr. E4d2 was eluted on a silica gel column and then purified by reversed-phase high performance liquid chromatography (HPLC) (MeCN–H_2O, 50/50, 2 mL·min^{-1}) to yield **2** (t_R = 37.6 min, 2.6 mg) and **3** (t_R = 31.1 min 2.6 mg). Fr. E4d4 was eluted on a silica gel column and subsequently purified by reversed-phase HPLC (MeCN–H_2O, 54/46, 2 mL·min^{-1}) to yield **4** (t_R = 18.9 min, 2.4 mg) and **5** (t_R = 27.2 min, 3.9 mg).

*Diphenylemestrin A (**1**):* yellow amorphous solid, $[\alpha]_D^{20}$ −320 (*c* 0.1, MeOH); UV (MeOH) λ_{max} (log ε) 264 (4.13); ECD (MeOH) λ_{max} $\Delta\varepsilon$ 227 (−46.7), 249 (+6.9), 300 (−4.0) nm; ^{1}H and ^{13}C NMR data (DMSO-d_6) see Tables S1 and S2; IR (KBr) ν_{max} 3420, 2955, 2920, 2851, 1693, 1656, 1605, 1517, 1461, 1382, and 1292 cm^{-1}; HR-ESI-MS [M + Na]$^+$ *m/z* 803.2043 (Calcd. for $C_{41}H_{36}N_2O_{14}Na^+$, 803.2064).

*Diphenylemestrin B (**2**):* yellow amorphous solid**,** $[\alpha]_D^{20}$ −588 (*c* 0.1, MeOH); UV (MeOH) λ_{max} (log ε) 266 (4.40); ECD (MeOH) λ_{max} $\Delta\varepsilon$ 221 (−37.3), 249 (+1.24), 270 (+7.3), 301 (−7.5) nm; ^{1}H and ^{13}C NMR data (DMSO-d_6) see Tables S1 and S2; IR (KBr) ν_{max} 3427, 2925, 2852, 1682, 1611, 1515, 1487, 1425, and 1384 cm^{-1}; HR-ESI-MS [M + Na]$^+$ *m/z* 785.1966 (Calcd. for $C_{41}H_{34}N_2O_{13}Na^+$, 785.1959).

*Diphenylemestrin C (**3**):* yellow amorphous solid, $[\alpha]_D^{20}$ −485 (*c* 0.1, MeOH); UV (MeOH) λ_{max} (log ε) 263 (4.28); ECD (MeOH) λ_{max} $\Delta\varepsilon$ 218 (−34.0), 249 (+0.5), 267 (+0.6), 311 (−6.2) nm; ^{1}H and ^{13}C NMR data (DMSO-d_6) see Tables S1 and S2; IR (KBr) ν_{max} 3426, 2926, 2851, 1713, 1686, 1610, 1515, 1463, and 1383 cm^{-1}; HR-ESI-MS [M + Na]$^+$ *m/z* 769.2031 (Calcd. for $C_{41}H_{34}N_2O_{12}Na^+$, 769.2009).

*Diphenylemestrin D (**4**):* yellow amorphous solid**,** $[\alpha]_D^{20}$ −165 (*c* 0.1, MeOH); UV (MeOH) λ_{max} (log ε) 307 (3.97), 264 (4.11); ECD (MeOH) λ_{max} $\Delta\varepsilon$ 228 (−19.0), 249 (+3.5), 300 (−2.8) nm; ^{1}H and ^{13}C NMR data (CD_3OD) see Tables S1 and S2; IR (KBr) ν_{max} 3432, 2925, 2851, 1678, 1657, 1608, 1516, 1445, 11405, and 1383 cm^{-1}; HR-ESI-MS [M + Na]$^+$ *m/z* 801.1891 (Calcd. for $C_{41}H_{34}N_2O_{14}Na^+$, 801.1908).

*Diphenylemestrin E (**5**):* yellow amorphous solid, $[\alpha]_D^{20}$ −144 (*c* 0.1, MeOH); UV (MeOH) λ_{max} (log ε) 261 (4.20), 239 (4.63); ECD (MeOH) λ_{max} $\Delta\varepsilon$ 228 (−22.7), 249 (+5.4), 306 (−1.7) nm; ^{1}H and ^{13}C NMR data (CD_3OD) see Tables S1 and S2; IR (KBr) ν_{max} 3430, 2925, 2852, 1678, 1605, 1514, 1477, 1441, and 1383 cm^{-1}; HR-ESI-MS [M + Na]$^+$ *m/z* 817.1876 (Calcd. for $C_{41}H_{34}N_2O_{15}Na^+$, 817.1857).

4.4. ECD calculations

The comprehensive methodology and procedures for ECD calculations of compound **1** are delineated in the Supporting Information.

4.5. Cytotoxicity assay

The cytotoxic effects of diphenylemestrins A–E (**1**–**5**) were assessed against the human cancer cell lines NB4, RKO, A549, SU-DHL-2, HEPG2, and HL60. All assays were conducted according to previously described protocols [34]. To prevent activity degradation, stock solutions of these compounds were prepared immediately prior to use and utilized promptly.

4.6. Immunosuppressive assay

Splenic lymphocytes were prepared as previously desc ribed [35]. The prepared spleen cells were cultured at 2.5 × 10^5 cells/well in 96-well round-bottom plates (Costar, Cambridge, MA, USA) containing 200 μL of RPMI-1640 medium with 10% heat-inactivated FBS. FK506, a clinical immunosuppressant, served as a positive control. Test compounds at various concentrations (0, 0.01, 0.1, 1, 2.5, 5, and 10 μmol·L^{-1}) and ConA (Sigma, USA) (5 μg·mL^{-1}) were added to T cells as selective stimuli. The plates were then incubated in a humidified chamber at 5% CO_2 and 37 °C. After 72 h, the CFSE signal of gated cells was measured using a FACS Celesta flow cytometer (BD, New Jersey, USA). The IC_{50} value was calculated using Origin 8.0 software from the nonlinear curve fitting of the percentage of inhibition versus the logarithm of the inhibitor concentration.

4.7. Anti-inflammatory assay

RAW264.7 cells were seeded into 96-well cell culture plates (5 × 10^3 cells/well) and exposed to compounds at concentrations ranging from 40 to 0.2 μmol·L^{-1} for 2 h, followed by induction with LPS (1 μg·mL^{-1}) for an additional 12 h. Dexamethasone, an anti-inflammatory drug, served as a positive control. NO accumulation in the culture medium was quantified using Griess reagent at 540 nm with a microplate reader.

4.8. Apoptosis assay

Cell apoptosis was assessed using the Annexin V-FITC/PI Apoptosis Kit (Elabscience, Wuhan, China). NB4 cells were seeded into 12-well plates (2 × 10^4 cells/well) and exposed to the compounds for 24 h. Prior to analysis, cells were suspended in a binding buffer containing Annexin V-FITC and PI probes and incubated for 10 min in darkness. Cell apoptosis was subsequently detected using a BD C6 flow cytometer (BD, New Jersey, USA) and analyzed using FlowJo software.

4.9. Measurement of mitochondrial membrane potential (MMP)

Intracellular mitochondrial membrane potential was assessed using the Elabscience® Mitochondrial Membrane Potential Assay Kit (with JC-1). Briefly, NB4 cells were seeded into 12-well plates (2 × 10^4 cells/well) and exposed to the compounds for 24 h. Subsequently, cells were suspended in JC-1 working solution and incubated for 20 min at 37 °C in darkness. The mitochondrial membrane potential was observed and captured using a fluorescence microscope (Olympus CKX53, Tokyo, Japan) and quantified by flow cytometry C6.

4.10. Western blot analysis

Western blot analysis of the apoptosis-related proteins in NB4 cells was conducted as previously described. Following a 24-hour treatment with compounds, cells were lysed in RIPA buffer containing Cocktail and PMSF. Protein quantification and equalization were performed using a BCA Kit (Beyotime, Shanghai, China). The proteins were separated on 10% or 15% SDS-PAGE gels and subsequently transferred to NC membranes. After blocking with 5% skim milk and washing with TBST, the membranes were incubated with primary antibodies against PARP, cleaved-caspase 3, and β-Actin overnight at 4 °C, followed by incubation

with fluorescent secondary antibodies. Protein bands were visualized using a two-color near-infrared fluorescence imaging system (LI-COR, Nebraska, USA).

Funding

This work was supported by The National Key Research and Development Program of China (No. 2021YFA0910500), the National Natural Science Foundation of China (Nos. U22A20380, 82104028, 82173706, and 82373755); the Science and Technology Major Project of Hubei Province (No. 2021ACA012), the Fundamental Research Funds for the Central Universities, HUST (No. 2021JYCXJJ058).

Availability of supporting information

Supporting information for this work can be obtained by contacting the corresponding authors *via* E-mail.

Declaration of competing interest

These authors have no conflict of interest to declare.

References

1 Ahuja M, Chiang YM, Chang SL, et al. Illuminating the diversity of aromatic polyketide synthases in *Aspergillus nidulans*. *J Am Chem Soc*. 2012;134(19): 8212-8221. https://doi.org/10.1021/ja3016395.
2 Lin H, Lyu H, Zhou S, et al. Deletion of a global regulator LaeB leads to the discovery of novel polyketides in *Aspergillus nidulans*. *Org Biomol Chem*. 2018;16(27):4973-4976. https://doi.org/10.1039/C8OB01326H.
3 An CY, Li XM, Luo H, et al. 4-Phenyl-3, 4-dihydroquinolone derivatives from *Aspergillus nidulans* MA-143, an endophytic fungus isolated from the mangrove plant *Rhizophora stylosa*. *J Nat Prod*. 2013;76(10):1896-1901. https://doi.org/10.1021/np4004646.
4 Scherlach K, Hertweck C. Discovery of aspoquinolones A–D, prenylated quinoline-2-one alkaloids from *Aspergillus nidulans*, motivated by genome mining. *Org Biomol Chem*. 2006;4(18):3517-3520. https://doi.org/10.1039/B607011F.
5 An CY, Li XM, Li CS, et al. Aniquinazolines A–D, four new quinazolinone alkaloids from marine-derived endophytic fungus *Aspergillus nidulans*. *Mar Drugs*. 2013;11(7):2682-2694. https://doi.org/10.3390/md11072682.
6 Lo HC, Entwistle R, Guo CJ, et al. Two separate gene clusters encode the biosynthetic pathway for the meroterpenoids austinol and dehydroaustinol in *Aspergillus nidulans*. *J Am Chem Soc*. 2012;134(10):4709-4720. https://doi.org/10.1021/ja209809t.
7 Zhang P, Li XM, Li X, et al. New indole-diterpenoids from the algal-associated fungus *Aspergillus nidulans*. *Phytochem Lett*. 2015;12:182-185. https://doi.org/10.1016/j.phytol.2015.03.017.
8 Bromann K, Toivari M, Viljanen K, et al. Engineering *Aspergillus nidulans* for heterologous ent-kaurene and gamma-terpinene production. *Appl Microbiol Biotechnol*. 2016;100(14):6345-6359. https://doi.org/10.1007/s00253-016-7517-5.
9 Sanchez JF, Entwistle R, Corcoran D, et al. Identification and molecular genetic analysis of the cichorine gene cluster in *Aspergillus nidulans*. *Med Chem Commun*. 2012;3(8):997-1002. https://doi.org/10.1039/c2md20055d.
10 Scherlach K, Schuemann J, Dahse HM, et al. Aspernidine A and B, prenylated isoindolinone alkaloids from the model fungus *Aspergillus nidulans*. *J Antibiot*. 2010;63(7):375-377. https://doi.org/10.1038/ja.2010.46.
11 Yeh HH, Chiang YM, Entwistle R, et al. Molecular genetic analysis reveals that a nonribosomal peptide synthetase-like (NRPS-like) gene in *Aspergillus nidulans* is responsible for microperfuranone biosynthesis. *Appl Microbiol Biotechnol*. 2012;96(3):739-748. https://doi.org/10.1007/s00253-012-4098-9.
12 Lin TS, Chen B, Chiang YM, et al. Discovery and elucidation of the biosynthesis of aspernidgulenes: novel polyenes from *Aspergillus Nidulans* by using serial promoter replacement. *ChemBioChem*. 2019;20(3):329-334. https://doi.org/10.1002/cbic.201800486.
13 Oakley CE, Ahuja M, Sun WW, et al. Discovery of McrA, a master regulator of *Aspergillus* secondary metabolism. *Mol Microbiol*. 2017;103(2):347-365. https://doi.org/10.1111/mmi.13562.
14 Wortman JR, Gilsenan JM, Joardar V, et al. The 2008 update of the *Aspergillus nidulans* genome annotation: a community effort. *Fungal Genet Biol*. 2009;46 (1,Supplement):S2-S13. https://doi.org/10.1016/j.fgb.2008.12.003.
15 Cerqueira GC, Arnaud MB, Inglis DO, et al. The *Aspergillus* genome database: multispecies curation and incorporation of RNA-Seq data to improve structural gene annotations. *Nucleic Acids Res*. 2014;42(D1):D705-D710. https://doi.org/10.1093/nar/gkt1029.
16 Welch TR, Williams RM. Epidithiodioxopiperazines. occurrence, synthesis and biogenesis. *Nat Prod Rep*. 2014;31(10):1376-1404. https://doi.org/10.1039/C3NP70097F.
17 Seya H, Nozawa K, Nakajima S, et al. Studies on fungal products. Part 8. Isolation and structure of emestrin, a novel antifungal macrocyclic epidithiodioxopiperazine from *Emericella striata*. X-Ray molecular structure of emestrin. *J Chem Soc, Perkin trans 1*. 1986(0):109-116.
18 Li Y, Yue Q, Krausert NM, et al. Emestrins: anti-cryptococcus epipolythiodioxopiperazines from *Podospora australis*. *J Nat Prod*. 2016; 79(9):2357-2363. https://doi.org/10.1021/acs.jnatprod.6b00498.
19 Herath KB, Jayasuriya H, Ondeyka JG, et al. Isolation and structures of novel fungal metabolites as chemokine receptor (CCR2) antagonists. *J Antibiot*. 2005;58(11):686-694. https://doi.org/10.1038/ja.2005.94.
20 Onodera H, Hasegawa A, Tsumagari N, et al. MPC1001 and Its analogues: new antitumor agents from the fungus *Cladorrhinum* species. *Org Lett*. 2004; 6(22):4101-4104. https://doi.org/10.1021/ol048202d.
21 Nozawa K, Udagawa SI, Nakajima S, et al. Studies on fungal products. XIV. emestrin B, a new epitrithiodioxopiperazine, from *Emericella striata*. *Chem Pharm Bull*. 1987;35(8):3460-3463. https://doi.org/10.1248/cpb.35.3460.
22 Li Q, Chen CM, Wei MS, et al. Niduterpenoids A and B: two sesterterpenoids with a highly congested hexacyclic 5/5/5/5/3/5 ring system from the fungus *Aspergillus nidulans*. *Org Lett*. 2019;21(7):2290-2293. https://doi.org/10.1021/acs.orglett.9b00581.
23 Li Q, Chen CM, He Y, et al. Prenylated quinolinone alkaloids and prenylated isoindolinone alkaloids from the fungus *Aspergillus nidulans*. *Phytochemistry*. 2020;169:112177. https://doi.org/10.1016/j.phytochem.2019.112177.
24 Li Q, Zheng YY, Fu AM, et al. 30-norlanostane triterpenoids and steroid derivatives from the endophytic fungus *Aspergillus nidulans*. *Phytochemistry*. 2022;201:113257. https://doi.org/10.1016/j.phytochem.2022.113257.
25 Fu AM, Chen CM, Li Q, et al. Niduenes A–F, six functionalized sesterterpenoids with a pentacyclic 5/5/5/5/6 skeleton from endophytic fungus *Aspergillus nidulans*. *Chin Chem Lett*. 2024;35(9): 109100. https://doi.org/10.1016/j.cclet.2023.109100.
26 Bode HB, Bethe B, Höfs R, et al. Big effects from small changes: possible ways to explore nature's chemical diversity. *ChemBioChem*. 2002;3(7):619-627. https://doi.org/10.1002/1439-7633(20020703)3:7<619::AID-CBIC619>3.0.CO;2-9.
27 Hu ZX, Ye Y, Zhang YH. Large-scale culture as a complementary and practical method for discovering natural products with novel skeletons. *Nat Prod Rep*. 2021;38(10):1775-1793. https://doi.org/10.1039/D0NP00069H.
28 Seya H, Nakajima S, Kawai K, et al. Structure and absolute-configuration of emestrin, a new macrocyclic epidithiodioxopiperazine from *Emericella Striata*. *J Chem Soc, Chem commun*. 1985; 657-658.
29 Qi JZ, Wu J, Kang SJ, et al. The chemical structures, biosynthesis, and biological activities of secondary metabolites from the culinary-medicinal mushrooms of the genus Hericium: a review. *Chin J Nat Med*. 2024;22(8):676-698. https://doi.org/10.1016/S1875-5364(24)60590-X.
30 Li XB, Zhou YH, Zhu RX, et al. Identification and biological evaluation of secondary metabolites from the endolichenic fungus *Aspergillus versicolor*. *Chem Biodivers*. 2015;12(4):575-592. https://doi.org/10.1002/cbdv.201400146.
31 Wang L, Dong JY, Song HC, et al. Screening and isolation of antibacterial activities of the fermentative extracts of freshwater fungi from Yunnan Province, China. *Ann Microbiol*. 2008;58(4):579-584. https://doi.org/10.1007/BF03175561.
32 Wang J, Chen M, Wang M, et al. The novel ER stress inducer Sec C triggers apoptosis by sulfating ER cysteine residues and degrading YAP *via* ER stress in pancreatic cancer cells. *Acta Pharm Sin B*, 2022, 12(1): 210-227.
33 Li, Q, Fu, A, Wei, M, et al. Asperemestrins A–D, emestrin hybrid polymers with bridged skeletons from the endophytic fungus *Aspergillus nidulans*. *Org Lett*. 2022; 24(37): 6800-6804. https://doi.org/10.1021/acs.orglett.2c02701.
34 Zhu H, Chen C, Tong Q, et al. Asperflavipine A: a cytochalasan heterotetramer uniquely defined by a highly complex tetradecacyclic ring system from *Aspergillus flavipes* QCS12. *Angew Chem Int Ed*. 2017;56(19):5242-5246. https://doi.org/10.1002/anie.201701125.
35 Lin S, He Y, Li F, et al. Structurally diverse and bioactive alkaloids from an insect-derived fungus *Neosartorya fischeri*. *Phytochemistry*. 2020;175: 112374. https://doi.org/10.1016/j.phytochem.2020.112374.